https://doi.org/10.5194/egusphere-2026-4809
Preprint. Discussion started: 20 August 2026

Quantifying and Predicting the Mesosphere and Lower Thermosphere Density during Austral Summer

Liang Zhang[1], Zhongfang Liu[1], Yajun Zhu[2]

[1]State Key Laboratory of Marine Geology, Tongji University, Shanghai, 200092, China
[2]State Key Laboratory of Solar Activity and Space Weather, National Space Science Center, Chinese Academy of Sciences, Beijing, 100190, China

Correspondence to: Liang Zhang (Liangzhang420@tongji.edu.cn)

Abstract. The mesosphere and lower thermosphere (MLT, 60-110 km) are a critical atmosphere-space transition layer, yet its density variability remains poorly quantified. Using 24 years (2002-2025) of the Sounding of the Atmosphere using Broadband Emission Radiometry (SABER) temperature measurements, we demonstrate that the T80 index—a temperature-based proxy at 80 km for the strength of austral summer polar upwelling—dominates MLT density fluctuations. A distinct vertical density dipole emerges over southern high latitudes: stronger upwelling (lower T80) increases density below 77 km via adiabatic cooling, yet substantially reduces density from 83 to 105 km. This dipole peaks near 95 km with a correlation of R = 0.98 and a sensitivity of 3.1% K^{-1}, jointly shaped by the column adjustment effect and the local thermal effect. Mirroring this high-latitude response, a weaker, negative correlation (peak R = -0.8, -0.5% K^{-1}) appears over low latitudes (55°S-35°N, 80-90 km), establishing an interhemispherically anti-phase density pattern driven by the same upwelling. The T80-density relationship remains robust on daily timescales, with a mean correlation of 0.78 (1.7% K^{-1}) at 80°S, 95 km. Owing to the strong month-to-month persistence of polar upwelling, the T80 index enables one-month-ahead MLT density predictions with a peak correlation of 0.90. Our results indicate that internal dynamical forcing from summer polar upwelling dominates interannual MLT density variability, while signals from the 11-year solar cycle and long-term CO_2 cooling cannot be reliably isolated from the 24-year observations.

1 Introduction

The mesosphere and lower thermosphere form a critical layer between the lower terrestrial atmosphere and near-Earth space. Its thermal, dynamical, and chemical states are jointly regulated by two distinct forcing pathways: top-down space weather drivers including solar irradiance and geomagnetic energy deposition, and bottom-up wave activities including gravity waves, planetary waves, and tides (Plane *et al.*, 2023; Vincent, 2015). This complexity has long hindered a comprehensive understanding of the MLT, particularly regarding the nature and causes of its density variability. Quantifying and predicting

https://doi.org/10.5194/egusphere-2026-4809
Preprint. Discussion started: 20 August 2026

MLT density is not only a scientific imperative for understanding atmospheric coupling but also a practical necessity for satellite drag modeling and orbit determination.

Long-term, continuous measurements of MLT density remain sparse (Baron *et al.*, 2020), limiting our ability to characterize its global structure and variability. In recent decades, physics-based empirical models (Emmert *et al.*, 2021) and deep learning approaches (Li *et al.*, 2026) have advanced rapidly. Meanwhile, a growing network of ground-based meteor radars provides valuable regional density retrievals between 85-95 km based on ambipolar diffusion (Yi *et al.*, 2023; Yi *et al.*, 2019; Yi *et al.*, 2018b; Younger *et al.*, 2015).

Existing studies have primarily focused on external forcings. The energy budget of the MLT is influenced by solar activity and geomagnetic storms, which induce significant temperature perturbations at both high and low latitudes, directly through Joule heating and energetic particle precipitation and indirectly through chemical and adiabatic dynamical processes (Li *et al.*, 2025; Liu *et al.*, 2025; Sun *et al.*, 2025). These temperature changes, in turn, may drive density variations. Meteor radar observations have detected MLT density responses to solar winds and geomagnetic storms (Yi *et al.*, 2018a; Yi *et al.*, 2017a; Yi *et al.*, 2017b). Similarly, SABER neutral density data have been used to analyze storm-time MLT density responses to an extreme geomagnetic storm, revealing that atmospheric expansion and uplift driven by temperature variations are the primary factors underlying the observed density change (Huang *et al.*, 2025). On longer timescales, a well-established CO_2-induced cooling trend is known to cause a long-term contraction of the middle atmosphere (Feofilov and Kutepov, 2012; Laštovička, 2017; Roble and Dickinson, 1989; Zhao *et al.*, 2020), with observable consequences such as decreasing mesospheric thickness, metal layers, meteor peak heights, and phase heights (Dawkins *et al.*, 2023; Mlynczak *et al.*, 2022; Peters *et al.*, 2017; She *et al.*, 2019). In addition, stratospheric sudden warmings also generate transient MLT density perturbations (Yang *et al.*, 2024).

In contrast to these external drivers, the internal atmospheric dynamics should play an important role in MLT density variability, yet relevant research remains limited. A prominent internal dynamical feature of the summertime MLT is gravity-wave-driven polar upwelling, which creates the coldest region in Earth's atmosphere with temperatures dropping to ~130 K (Garcia and Solomon, 1985; Holton, 1983; Lindzen, 1981). Our recent works introduced a temperature-based proxy for the intensity of this summer polar upwelling, termed the T80 index and defined as the zonal-mean temperature near 80 km over the summer polar region (Zhang and Liu, 2026; Zhang *et al.*, 2025c; Zhang *et al.*, 2026). Lower T80 values correspond to stronger upwelling, owing to adiabatic cooling. Based on the T80 index, we found that upwellings influence mesospheric chemistry and climate through a bottom-up mechanism involving water vapor (H_2O), oxygen (O), ozone (O_3; $O_x = O + O_3$), and temperature above 90 km (T90) (Zhang *et al.*, 2025b; Zhang *et al.*, 2025c).

During the austral summer months, the polar upwelling drives a vertical temperature dipole at the summer polar region. Specifically, stronger upwelling causes lower temperature below ~90 km via adiabatic cooling, and higher temperature above ~90 km through coupled dynamical, microphysical, chemical, and thermal processes via the bottom-up T80-H_2O-O_3-T90 chain (Zhang *et al.*, 2025c). This vertical temperature dipole alters the vertical temperature profile and lowers the cold-point mesopause height (Zhang *et al.*, 2026). Within the bottom-up mechanism, polar mesospheric clouds

https://doi.org/10.5194/egusphere-2026-4809
Preprint. Discussion started: 20 August 2026

(PMCs) play a key role. PMCs modulate H_2O distribution via a cold-trap effect, which hydrates the region below PMCs while it dehydrates the region above (Zhang *et al.*, 2025a; Zhang *et al.*, 2025c; Zhang *et al.*, 2022). The dehydration above PMCs increases O_x abundance (Siskind *et al.*, 2018), whose chemical and radiative heating (Wu *et al.*, 2026) further increases the temperature above summer polar mesopause. Concurrently, the meridional winds transport H_2O toward the winter hemisphere, causing O_x loss and lower temperature there. As a result, the mesospheric climate exhibits an interhemispheric anti-phase pattern during solstice months (Zhang *et al.*, 2025c). Thus, the summer polar upwelling, through this coupled bottom-up chain, emerges as a master regulator of the austral summer mesospheric climate.

Based on the above advances, the summer polar upwelling is expected to influence MLT neutral density via its temperature response. This study addresses three specific questions: (1) How does the T80 index influence the MLT density interannual variability on global scales? (2) What is the underlying physical mechanism linking the T80 index to MLT density changes? (3) Can the T80 index be used to build skillful one-month-ahead statistical forecasts of MLT density?

Using 24 years (2002-2025) of SABER density measurements, we systematically quantify the T80-density relationship on both interannual and daily timescales, propose column adjustment and local thermal effects as underlying mechanisms, and evaluate the subseasonal predictive skill based on the month-to-month persistence of T80 index. This work aims to elucidate the role of internal forcing (summer polar upwelling) on MLT density during austral summer, and assess whether external forcings (11-year solar cycle and long-term CO_2 cooling) can be detected within current observations.

2 Data and method

2.1 Multi-satellite observations

The SABER instrument aboard the NASA TIMED satellite (launched on 7 December 2001, 74.1° inclination) operates on a 60-day yaw cycle, alternating hemispheric coverage between 83°N-52°S and 52°N-83°S (Russell *et al.*, 1999). During the austral summer (November-January), the Southern Hemisphere (SH) high latitudes poleward of 52°S are optimally observed. We employ SABER version 2.07 level-2 temperature data spanning 2002-2025 (Remsberg *et al.*, 2008), which exhibit excellent long-term stability across the MLT region (Liu *et al.*, 2026; Mlynczak *et al.*, 2020). The SABER neutral density profiles are derived from its temperature and pressure profiles via the hydrostatic relation and ideal gas law. Despite being a secondary product, SABER density has been applied in geomagnetic storm analyses (Huang *et al.*, 2025), empirical model corrections (Cheng *et al.*, 2020), meteor radar comparisons (Yi *et al.*, 2018b), and turbopause identification (Wang *et al.*, 2025). In this study, each density profile is interpolated onto a 1 km vertical grid, and zonal means are computed to examine interannual and daily variability across latitudes.

The Microwave Limb Sounder (MLS) instrument aboard the Aura satellite, launched in 2004, provides nearly global coverage from 82°N to 82°S. We use MLS version 5 temperature data, with a typical single-profile precision of 3 K (Jiang *et al.*, 2007; Schwartz *et al.*, 2008). MLS offers robust, uninterrupted sampling over the austral summer high latitudes and therefore serves as the core dataset for constructing the T80 index. This study utilizes temperature measurements from

https://doi.org/10.5194/egusphere-2026-4809
Preprint. Discussion started: 20 August 2026

these two complementary satellite instruments, SABER and MLS, to construct a continuous, long-term (2002-2025) T80 index for interannual analysis.

2.2 The T80 index

Direct long-term measurements of mesospheric vertical winds are still unavailable, because summer polar upwelling speeds are typically only a few cm s^{-1} (Smith, 2012). We therefore employ the T80 index, defined as the zonal-mean temperature near 80 km over the summer polar region (Zhang and Liu, 2026; Zhang *et al.*, 2025c; Zhang *et al.*, 2026). This index serves as a robust proxy for the strength of mesospheric upwelling: a lower T80 value indicates stronger adiabatic cooling and thus stronger upwelling. The 80 km level is chosen for two reasons: (1) the extremely low ozone concentration at this altitude renders radiative and chemical heating negligible, such that temperature is dominated by adiabatic processes; (2) temperature measurements at this altitude show high cross-instrument consistency (García-Comas *et al.*, 2014), enabling reliable multi-satellite merging.

Constructing a continuous, long-term T80 time series requires reconciling the different observing patterns of SABER and MLS. SABER's yaw cycle introduces significant year-to-year variations in high-latitude coverage. Zhang *et al.* (2026) showed that full monthly December observations over 53°S-83°S are available before 2019, after which coverage gradually declines. November observation days increased from ~10 in 2002 to ~30 in 2019, while January days decreased from ~15 in 2003 to 0 in 2016 (Fig. 1 therein). Zhang *et al.* (2026) produced a fused T80 index time series (Table 1 therein) based primarily on the direct MLS T80 index (2004-2025), extended back to 2002-2003 using the calibrated SABER values. This fused T80 index is used throughout the present study.

3 Results

3.1 Climatology and interannual variability of austral summer MLT density

Figure 1 presents the December (austral summer) climatological mean and interannual standard deviation of MLT density, derived from 24 years (2002–2025) of SABER observations. The climatological mean field (Fig. 1a) reveals a pronounced latitudinal reversal in density structure across the MLT. In the lower layer (60–90 km), the summer high latitudes exhibit higher density than mid- and low-latitudes. This enhancement reflects the overall expansion of the atmospheric column driven by elevated tropospheric and stratospheric temperatures during austral summer. Above 95 km, however, the pattern reverses: the summer high-latitude upper MLT shows lower density than other latitudinal bands. This upper-level density depletion arises from persistent summer polar upwelling, which adiabatically cools the mesosphere and contracts the upper atmospheric column, thereby reducing local air density.

The interannual standard deviation (Fig. 1b) quantifies the year-to-year variability of December MLT density. The variability exhibits strong vertical and latitudinal dependence, with a pronounced maximum centered in the summer high-

https://doi.org/10.5194/egusphere-2026-4809
Preprint. Discussion started: 20 August 2026

latitude MLT between 85 km and 105 km. The peak occurs near 96 km, where the relative standard deviation reaches 17%. This identifies the summer polar upper MLT as the dominant region of interannual density variability during austral summer. Similar patterns are observed in November and January (not shown). Such prominent variability implies the existence of strong modulators governing the year-to-year density fluctuations at high latitudes, which motivates the T80-based analysis in the following sections.

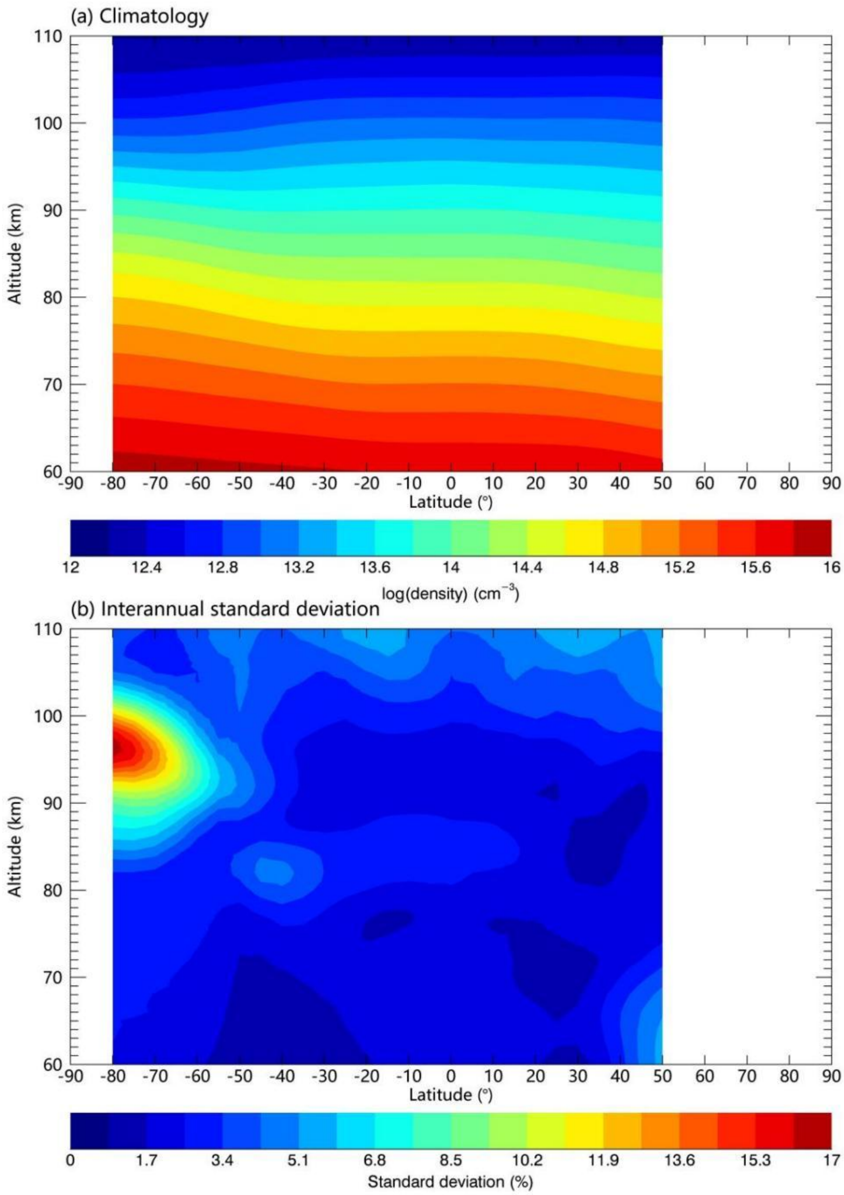

Figure 1. Climatological density distribution in December and the interannual standard deviation, based on SABER data (2002-2025).

https://doi.org/10.5194/egusphere-2026-4809
Preprint. Discussion started: 20 August 2026

3.2 The T80-density linkage on interannual scales

To quantify the interannual relationship between summer polar upwelling and MLT density, Fig. 2 presents concurrent December time series of the T80 index and density at 95 km and 80°S over 2002-2025. The T80 index (red) and high-latitude upper MLT density (blue) exhibit strong in-phase covariation, yielding a correlation coefficient of R = 0.98 and a positive density sensitivity of 3.1% K^{-1}. Both variables show interannual variability substantially larger than their long-term trends: the T80 index has an interannual standard deviation (σ) of 5.1 K and a positive trend of 1.5 K $decade^{-1}$, while the 95 km density varies by 15.9% (σ) with a positive trend of 6.4% $decade^{-1}$. Year-to-year oscillations thus dominate the temporal evolution of austral summer high-latitude upper MLT density.

Physically, the positive T80 trend (Fig. 2) indicates a gradual weakening of the summer polar upwelling over the 24-year record. A weaker upwelling reduces mesospheric adiabatic cooling and expands the atmospheric column, elevating neutral density at 95 km. This T80-driven density enhancement opposes the canonical expectation of CO_2-induced atmospheric contraction, implying that internal dynamical forcing overwhelms the long-term radiative cooling effect at these altitudes. This issue is revisited in Sect. 4.3.

In contrast to the high-latitude upper MLT, Fig. 3 shows an out-of-phase relationship between the T80 index and December MLT density at low latitudes (10°S, 83 km). The correlation is R = -0.80, with a sensitivity of -0.47% K^{-1}. The low-latitude density exhibits much weaker interannual variability (σ = 3.0%) and a slight negative trend (-1.03% $decade^{-1}$), opposite in sign to the high- latitude trend. These contrasting results confirm that the T80 index exerts a robust but latitude- and altitude-dependent modulation: positive density responses in the high-latitude upper MLT versus negative responses in the low-latitude mesosphere, with the latter being considerably weaker in magnitude.

To map the full spatial structure of the T80-density relationship, Fig. 4 presents altitude-latitude cross-sections of correlation coefficients (Fig. 4a) and linear regression sensitivities (Fig. 4b) for December, derived from 24-year (2002-2025) zonal-mean SABER monthly data. Over southern high latitudes (50°S-80°S), a clear vertical density dipole emerges (Fig. 4a). Density is negatively correlated with T80 below 77 km and strongly positively correlated between 83 km and 105 km, with peak R reaching 0.98—consistent with the pointwise time series in Fig. 2. Outside the polar band, significant negative correlations prevail across 80-90 km over 50°S-50°N, with maximum values up to -0.80, matching the low-latitude relationship in Fig. 3. Zhang *et al.* (2025c) demonstrated interhemispheric anti-phase temperature variability driven by summer polar upwelling (Fig. 4 therein). Similarly, Fig. 4a reveals a high-latitude vs. low-latitude anti-phase density variability, which will be further discussed in Sect. 4. The sensitivity field (Fig. 4b) quantifies the spatial heterogeneity of the density response. A strong positive sensitivity center (~3.0% K^{-1}) appears near 95 km over southern high latitudes, reflecting upper MLT density enhancement under weakened upwelling. In the lower high-latitude mesosphere near 70 km, the negative sensitivity is modest (-0.3% K^{-1}). Across mid-to-low latitudes, sensitivities are consistently weak (-0.5% K^{-1}) throughout 80-90 km, highlighting the weak thermal response away from the polar region. Fig. 5 extends the analysis to November and January, which closely resemble the December pattern.

https://doi.org/10.5194/egusphere-2026-4809
Preprint. Discussion started: 20 August 2026

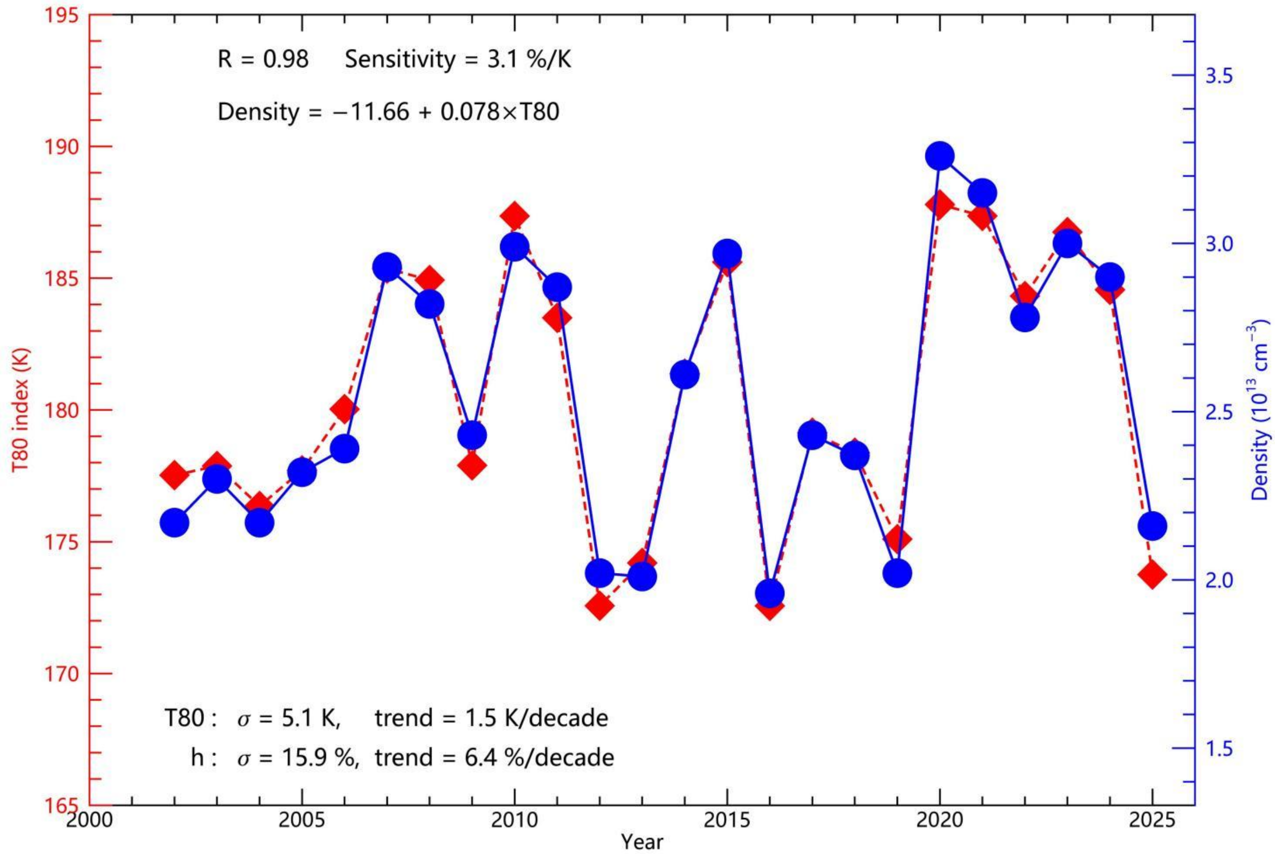

Figure 2. Dominant interannual control of the MLT density at 80°S, 95 km by the T80 index in December. The time series of the December T80 index (red) and the density (blue) demonstrate in-phase covariation. The correlation coefficient (R), linear regression equation, interannual standard deviations (σ), and decadal linear trends for both variables are annotated.

https://doi.org/10.5194/egusphere-2026-4809
Preprint. Discussion started: 20 August 2026

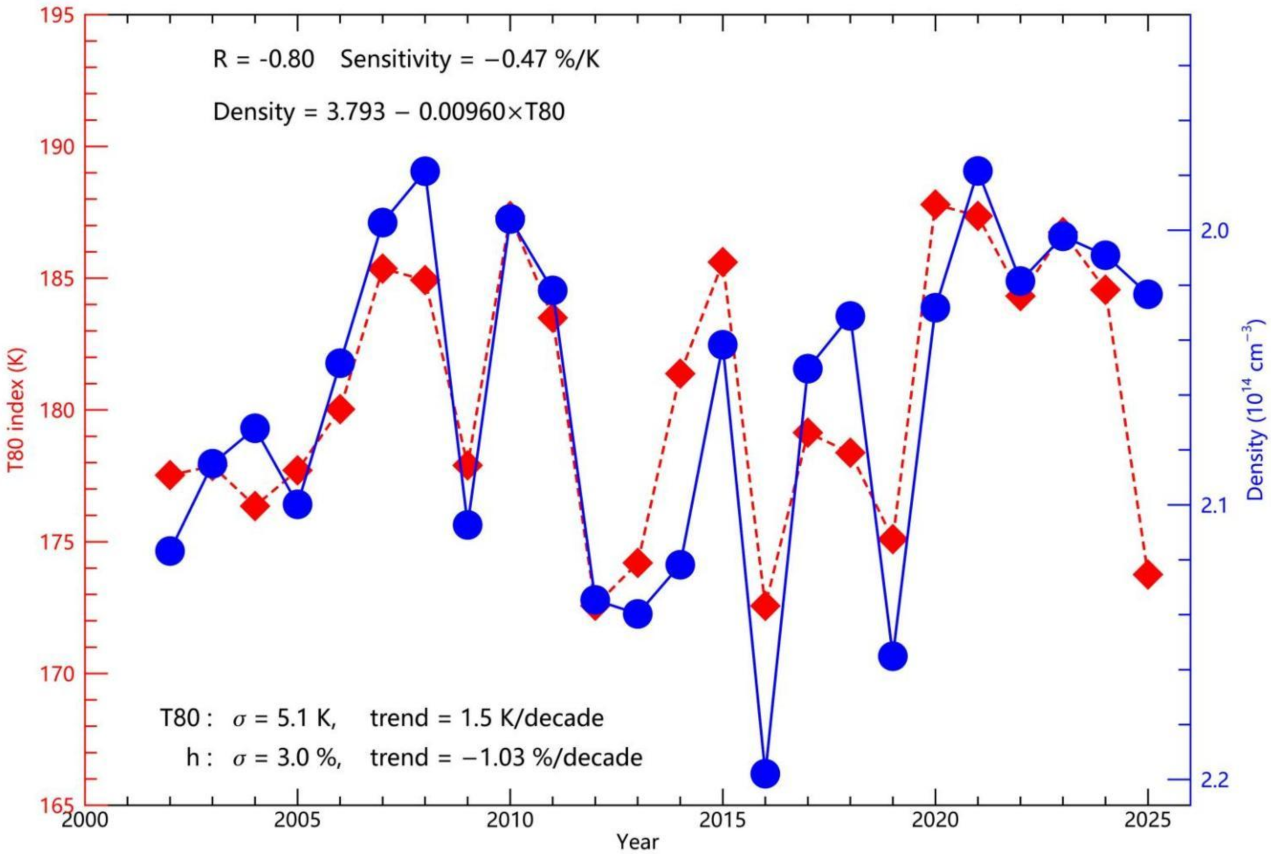

Figure 3. As in Fig. 2, but for the relationship of the MLT density at 10°S, 83 km with the T80 index in December.

https://doi.org/10.5194/egusphere-2026-4809
Preprint. Discussion started: 20 August 2026

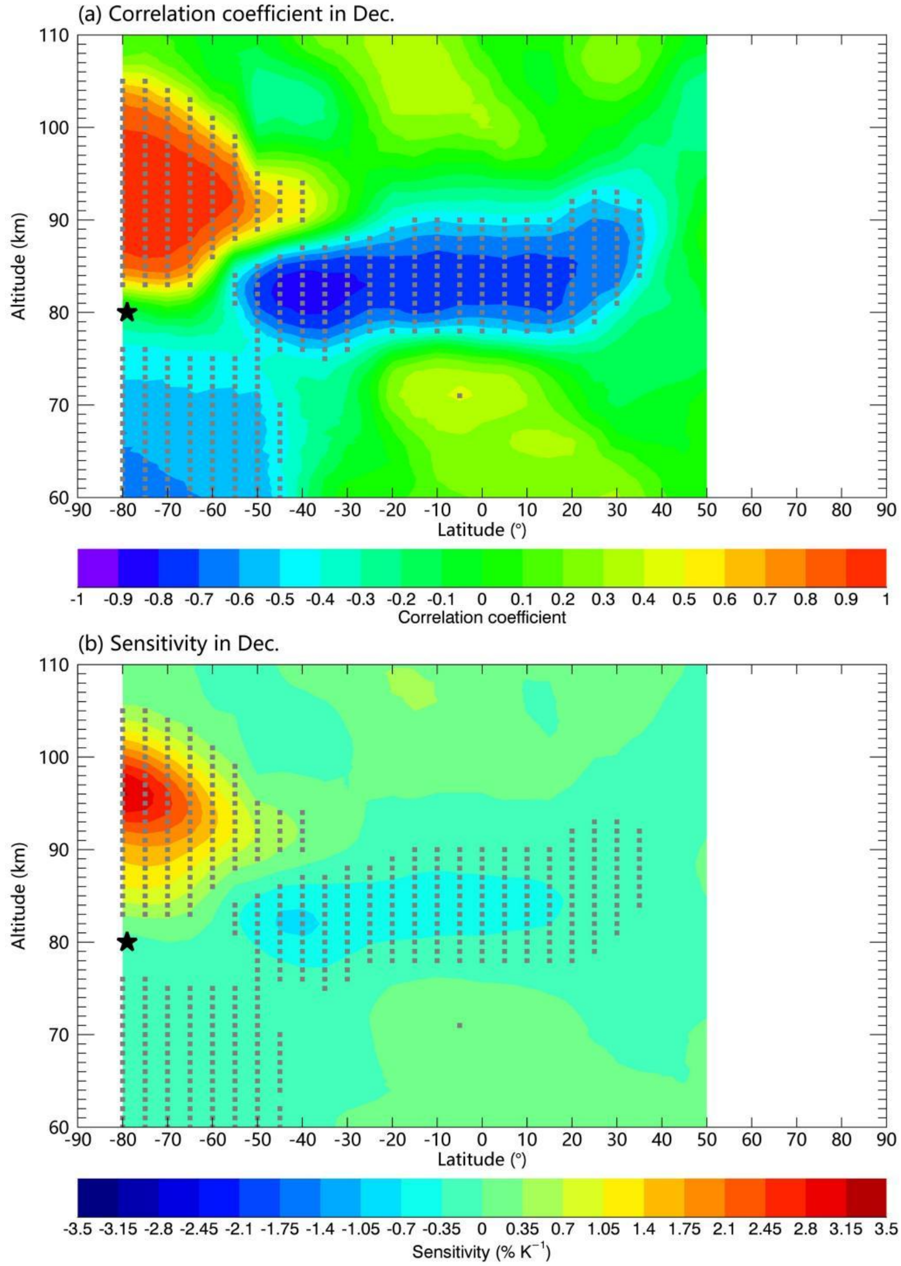

Figure 4. Latitudinal structure of the T80-density relationship in December. (a) The correlation coefficient and (b) the sensitivity between the T80 index and MLT density at varying latitudes. Gray points mark the 0.95 significant level. Sensitivity is obtained by linear regression. All data are monthly and zonal means from SABER observation during 2002-2025.

https://doi.org/10.5194/egusphere-2026-4809
Preprint. Discussion started: 20 August 2026

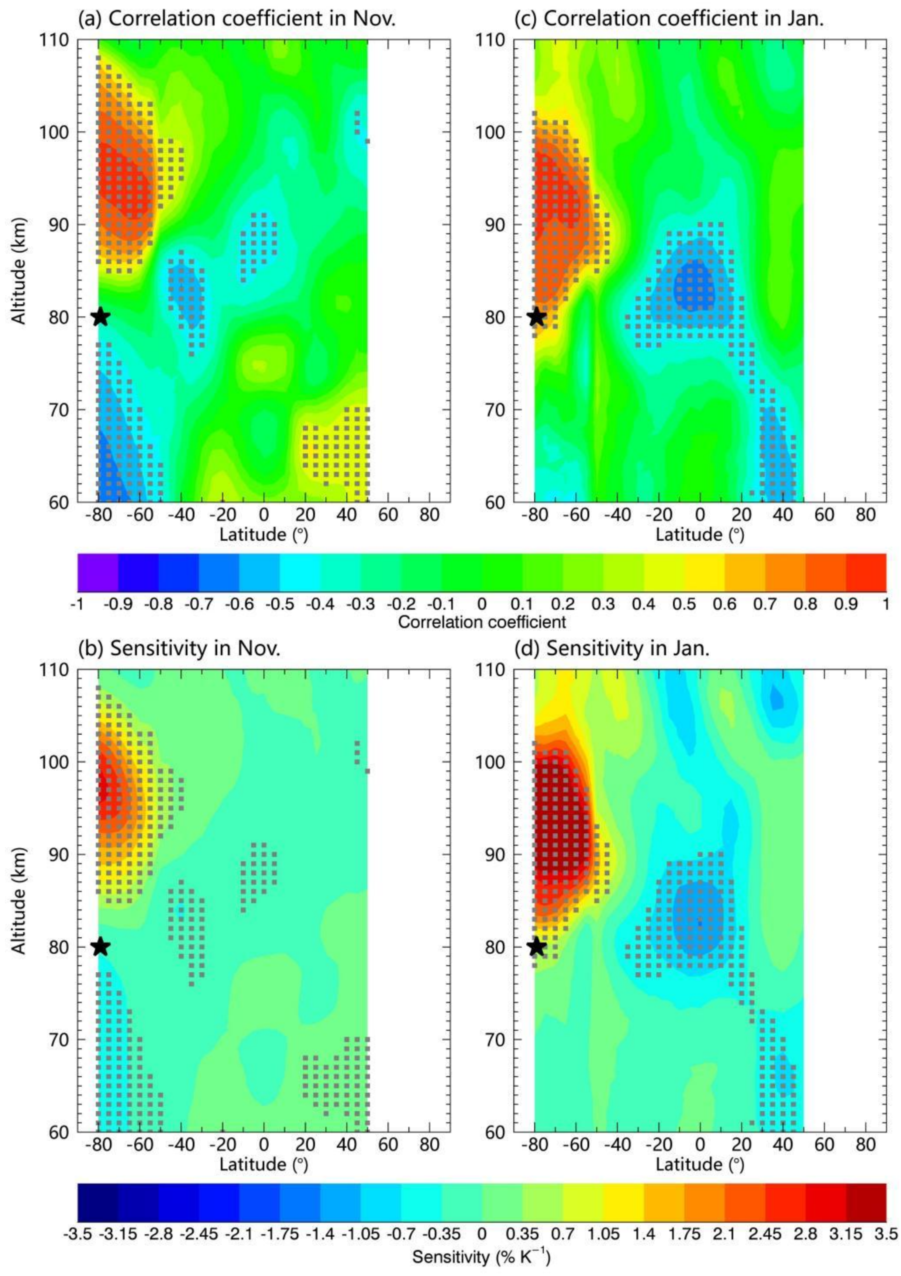

180 **Figure 5.** As in Fig. 4, but for November and January.

https://doi.org/10.5194/egusphere-2026-4809
Preprint. Discussion started: 20 August 2026

3.3 Statistical forecast of MLT density with one-month lead

The strong month-to-month persistence of the summer polar upwelling allows the T80 index to serve as a precursor for forecasting MLT density one month ahead. Fig. 6 shows the spatial distributions of predictive correlation and sensitivity for two forecast pairs: November T80 predicting December density, and December T80 predicting January density.

Figure 6 presents the November T80-December density forecast. The predictive skill originates from the high persistence of the T80 index between consecutive months (R = 0.90 for November-December). As a result, the predictive spatial pattern closely replicates the simultaneous T80-density relationship (Fig. 4). The classic vertical dipole of density response is well reproduced over southern high latitudes: negative predictive correlations at 60-75 km and strong positive correlations at 83-105 km. The predictive correlation reaches 0.90 at 80°S, 95 km, demonstrating excellent one-month forecast capability for the key high-latitude density variability. Across mid-to-low latitudes, significant negative predictive correlations persist in the 80-90 km mesosphere, consistent with the synchronous relationship. Similarly, the January MLT density can also be predicted by the T80 index in December, with correlation coefficients up to 0.80 (not shown).

Overall, the persistent summer polar upwelling signal enables skillful one-month-ahead prediction of MLT density anomalies. The close correspondence between the synchronous regression patterns and the one-month forecast patterns confirms that the T80 index is a reliable precursor for subseasonal prediction of austral summer MLT density.

https://doi.org/10.5194/egusphere-2026-4809
Preprint. Discussion started: 20 August 2026

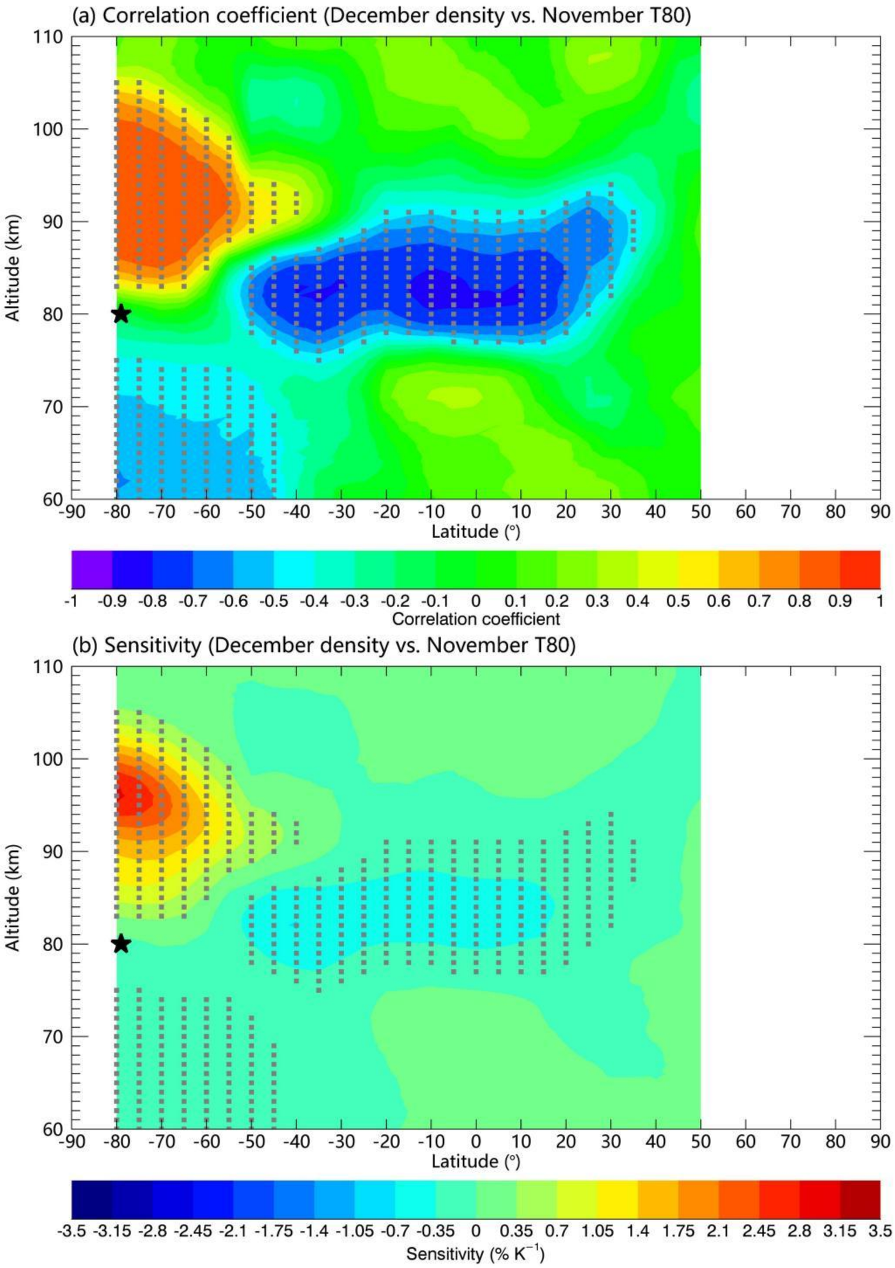

Figure 6. Prediction of December MLT density by the November T80 index with a lead time of one month. (a) The correlation coefficient and (b) the sensitivity. Gray points mark the 95% significant level.

https://doi.org/10.5194/egusphere-2026-4809
Preprint. Discussion started: 20 August 2026

3.4 The T80-density linkage on daily scales

The preceding sections have established the T80-density relationship on monthly-mean timescales. Here we assess whether this linkage also holds on daily timescales, which would confirm that the bottom-up mechanism operates not only climatically but also as a day-to-day dynamical process.

Figures 7 and 8 display the daily time series of the T80 index and the density at 80°S and 95 km for each austral summer from 2002 to 2025. The T80 index is calculated as the zonal and daily mean SABER temperature averaged between 75°S and 83°S at 80 km. Across all 24 years, the daily correlation between T80 and density at 95 km is consistently positive and statistically significant at the 95% confidence level. The 24-year mean daily correlation is R = 0.78, with eight individual years (2003, 2006, 2007, 2008, 2010, 2015, 2017, and 2024) exceeding 0.90, indicating that the T80-density linkage is a stable feature of the austral summer MLT.

Figure 9 presents the latitude-height cross-section of the daily-scale T80-density relationship, averaged over all 24 summers. Panel (a) shows the mean correlation coefficient, and panel (b) shows the mean regression sensitivity. The spatial pattern closely resembles that found for the monthly-mean data (Fig. 4). Over the summer high-latitude region (50°S-80°S), the vertical density dipole is clearly reproduced on daily timescales: negative correlation below ~83 km and strong positive correlation between 91 km and 104 km, with a peak mean daily correlation of approximately R = 0.81 near 96 km. The low-latitude negative band between 80 km and 90 km (50°S-50°N) is also present, with a peak negative correlation of approximately -0.60 near 10°S, 85 km. Although these daily correlation magnitudes are lower than their monthly counterparts (0.81 vs. 0.98 at the high-latitude peak; -0.60 vs. -0.80 at the low-latitude peak), the overall structure is preserved, confirming that the T80-density linkage is robust across temporal scales.

The daily sensitivity (Fig. 9b) at the high-latitude peak near 96 km, 80°S is approximately 2% K^{-1}, notably smaller than the monthly-mean sensitivity of 3.2% K^{-1} reported in Sect. 3.2. This reduction is expected: on daily timescales, additional high-frequency variability (e.g., from gravity waves, tides, and planetary waves) introduces noise that dilutes the T80 signal, whereas on monthly timescales such noise is effectively averaged out. Nevertheless, the daily correlation of 0.78 and sensitivity of 2% K^{-1} demonstrate that the T80 index captures a substantial fraction of the day-to-day density variability, making it a useful diagnostic even at weather-relevant timescales.

https://doi.org/10.5194/egusphere-2026-4809
Preprint. Discussion started: 20 August 2026

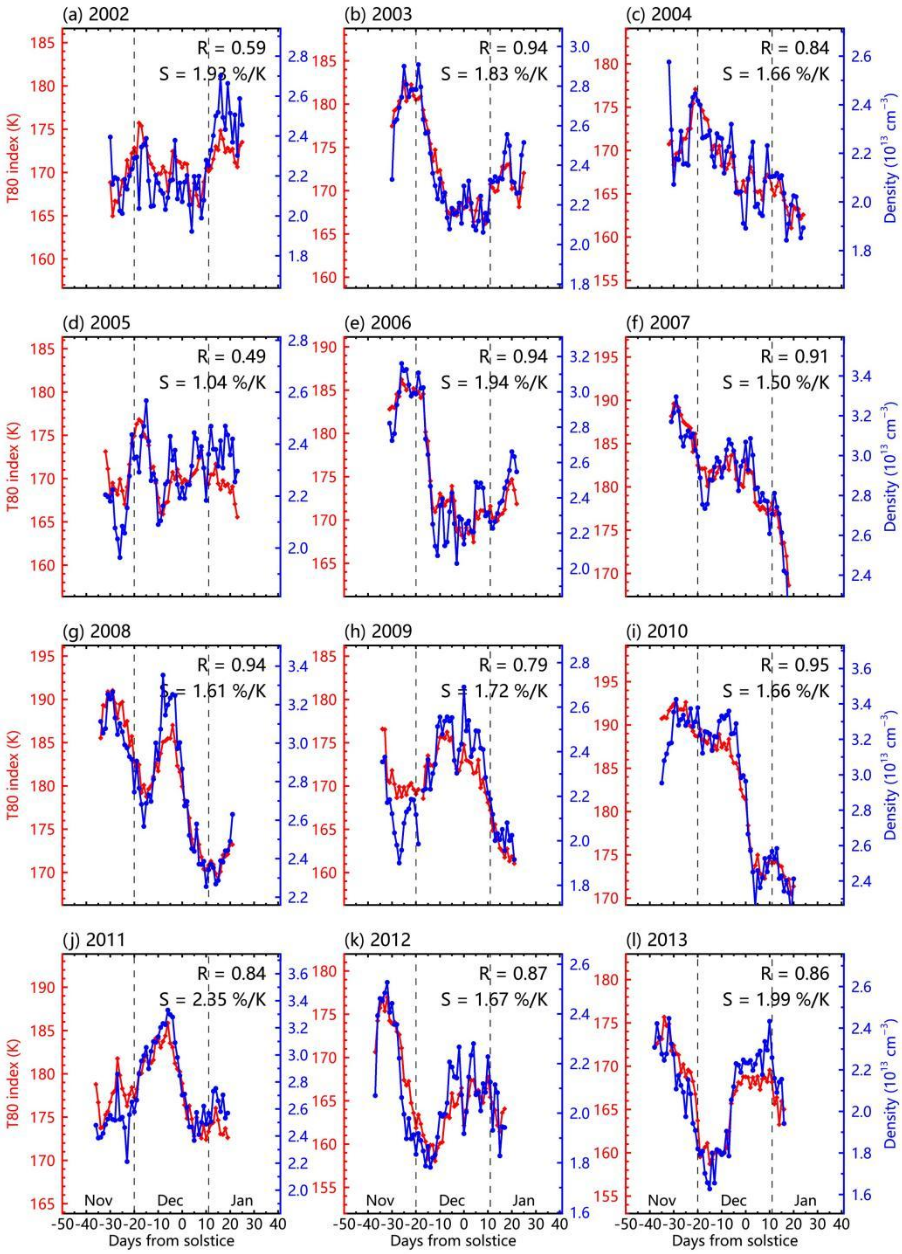

Figure 7. Daily-scale relationship between the T80 index and MLT density at 80°S, 95 km for each year from 2002 to 2013. The T80 index is the zonal and daily mean SABER temperature between 75°S and 83°S at ~80 km.

https://doi.org/10.5194/egusphere-2026-4809
Preprint. Discussion started: 20 August 2026

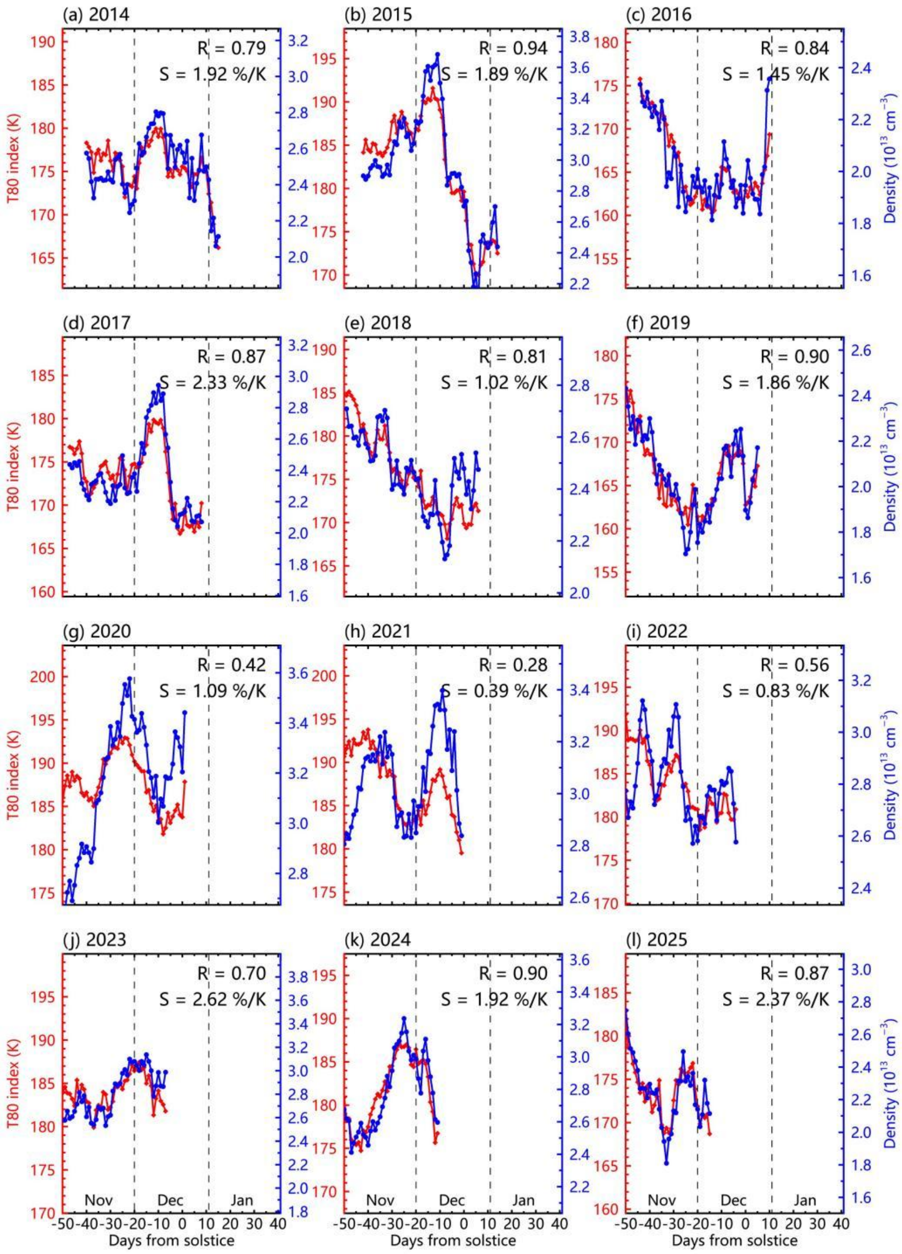

Figure 8. As in Fig. 7, but for the years 2014-2025.

https://doi.org/10.5194/egusphere-2026-4809
Preprint. Discussion started: 20 August 2026

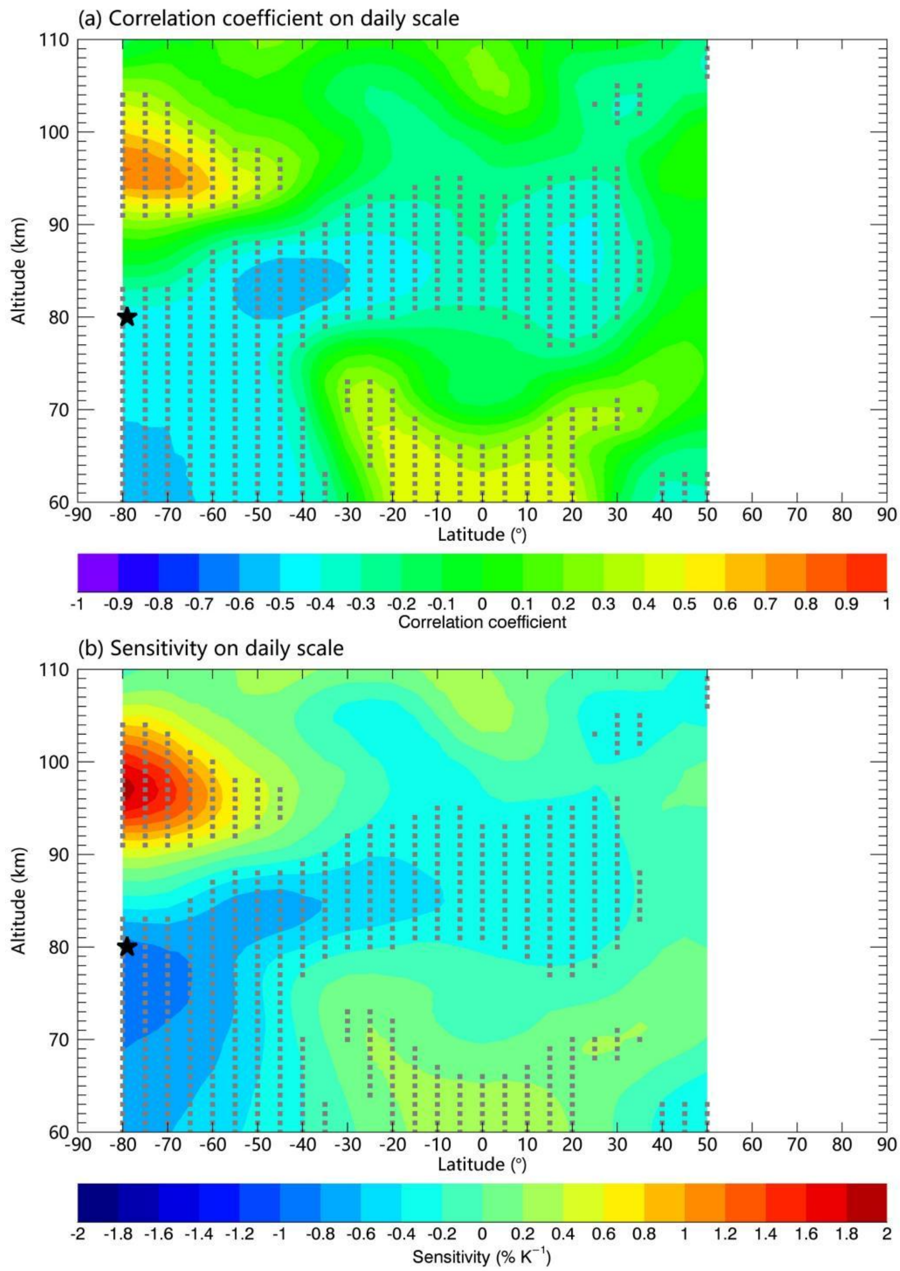

Figure 9. The daily-scale T80-density relationship, averaged over 2002-2025. (a) Mean correlation coefficient and (b) mean sensitivity (% K^{-1}) between the T80 index and density. Gray points indicate the 95% significant level.

https://doi.org/10.5194/egusphere-2026-4809
Preprint. Discussion started: 20 August 2026

4 Discussion

4.1 Mechanism: column adjustment effect and local thermal effect

The preceding results reveal a robust vertical density dipole over southern high latitudes and a uniform negative response at low latitudes, on both daily and interannual timescales. In particular, Figs. 4 and 9 show that the MLT density variability is interhemispherically anti-phase, similar to the latitudinal pattern of temperature variability (Zhang *et al.*, 2025c). Here we clarify the underlying physical mechanisms by separating two dominant processes: the column adjustment effect and the local thermal effect. In contrast to the conventional term "shrink effect", which refers to long-term CO_2-induced cooling and contraction (Lübken *et al.*, 2013), the column adjustment effect is an internal dynamical process describing the expansion or contraction of the lower atmospheric column driven by year-to-year perturbations in summer polar upwelling, rather than by radiative forcing.

Figure 10 presents vertical profiles of T80-related covariabilities at 80°S for December, including the T80-density relationship (Fig. 10a), the T80-temperature relationship (Fig. 10b), and the local temperature-density relationship (Fig. 10c). Fig. 10a shows a vertical density dipole consistent with the pattern in Fig. 4: density is negatively correlated with T80 below 77 km and positively correlated between 83 km and 105 km, with a transition near 81 km. Fig. 10b shows a vertical temperature dipole: T80 is positively correlated with local temperature below 91 km and negatively correlated above 93 km, with a transition near 92 km. Physically, stronger upwelling (lower T80) produces adiabatic cooling below 91 km and elevated temperatures above 93 km via chemical heating through the bottom-up mechanism (Zhang *et al.*, 2025c; Zhang *et al.*, 2026). Fig. 10c reveals three distinct vertical regimes for the local temperature-density relationship, arising from the joint modulation of the column adjustment effect and the local thermal effect.

(1) Lower mesosphere (70-80 km): Local temperature and density are negatively correlated. Stronger upwelling cools the local atmosphere and contracts the column, increasing local density. This regime is dominated by the local thermal effect.

(2) Transitional layer (85-91 km): An anomalous positive temperature-density correlation emerges from competition between the two mechanisms. The cooled, contracted subjacent column (below 82 km) reduces the air mass in this layer via column adjustment effect, tending to decrease density. Concurrently, local cooling acts to increase density via the local thermal effect. The column adjustment effect dominates, producing the counterintuitive positive temperature-density correlation and suppressing the net T80-density sensitivity in this layer (Fig. 10a).

(3) Upper MLT (93-105 km): The two mechanisms act cooperatively. Stronger upwelling elevates local temperature, thermally reducing density, while the persistent contraction of the lower column further amplifies this reduction. The superposition of cooperative effects produces the extremely strong T80-density correlation (R reaching 0.98) and the maximum sensitivity of 3.2% K^{-1} near 95 km, explaining the dominant interannual variability center in the summer polar upper MLT (Fig. 1).

https://doi.org/10.5194/egusphere-2026-4809
Preprint. Discussion started: 20 August 2026

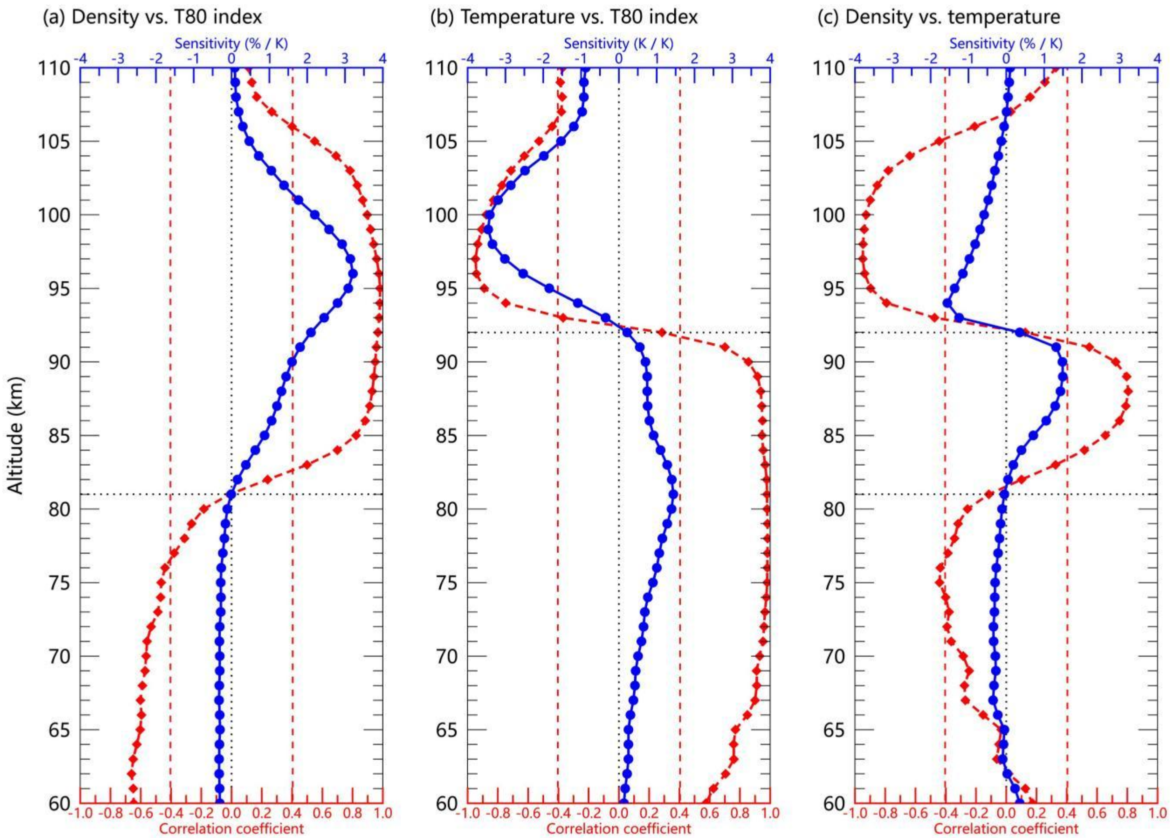

Figure 10. Mechanism of the T80 upwelling index modulating the MLT density at 80°S in December on interannual timescales. (a) Correlation coefficients (red) and sensitivity (blue) of density at varying altitudes to the T80 index. (b) Correlation coefficients (red) and sensitivity (blue) of temperature at varying altitudes to the T80 index. (c) Correlation coefficients (red) and sensitivity (blue) of density at varying altitudes to local temperature. Dashed lines mark the 95% significant level for the correlation coefficients.

4.2 Density variability at low latitudes

Figure 11 reveals the latitude-altitude structure of the T80-temperature relationship. The temperatures between 80-90 km are positively correlated with T80 index, consistent with the bottom-up mechanism (Zhang *et al.*, 2025c). Specifically, intensified summer polar upwelling (lower T80) enhances equatorward transport of H_2O from the polar region. The increased H_2O reduces O and O_3 abundances through ozone catalytic cycles, and the consequent reduction in O_x heating lowers the low-latitude temperatures. Conversely, the temperatures between 45°S and 25°N, at 68-78 km are negatively correlated with the T80 index. Zhang *et al.* (2025c) also found H_2O and temperature responses at low latitudes below 80 km (Fig. 4 therein), but did not provide an explanation. Here we hypothesize that this negative correlation may arise from a downwelling in the tropical region below 80 km induced by summer polar upwelling to satisfy mass conservation.

However, Fig. 11b shows that the sensitivity of low-latitude temperatures to the T80 index is only about 0.5 K K^{-1} between 80-90 km and about -0.5 K K^{-1} between 68-78 km, much smaller than that at high latitudes (-3.0 K K^{-1}). The correlation coefficients at low latitudes are also weaker. As a result, the sensitivity of low-latitude density to the T80 index is also weak. Fig. 4 shows that the density at 55°S-35°N and 78-91 km is significantly negatively correlated with the T80 index (about -0.5% K^{-1}), but there is no such vertical density dipole structure as seen at high latitudes.

https://doi.org/10.5194/egusphere-2026-4809
Preprint. Discussion started: 20 August 2026

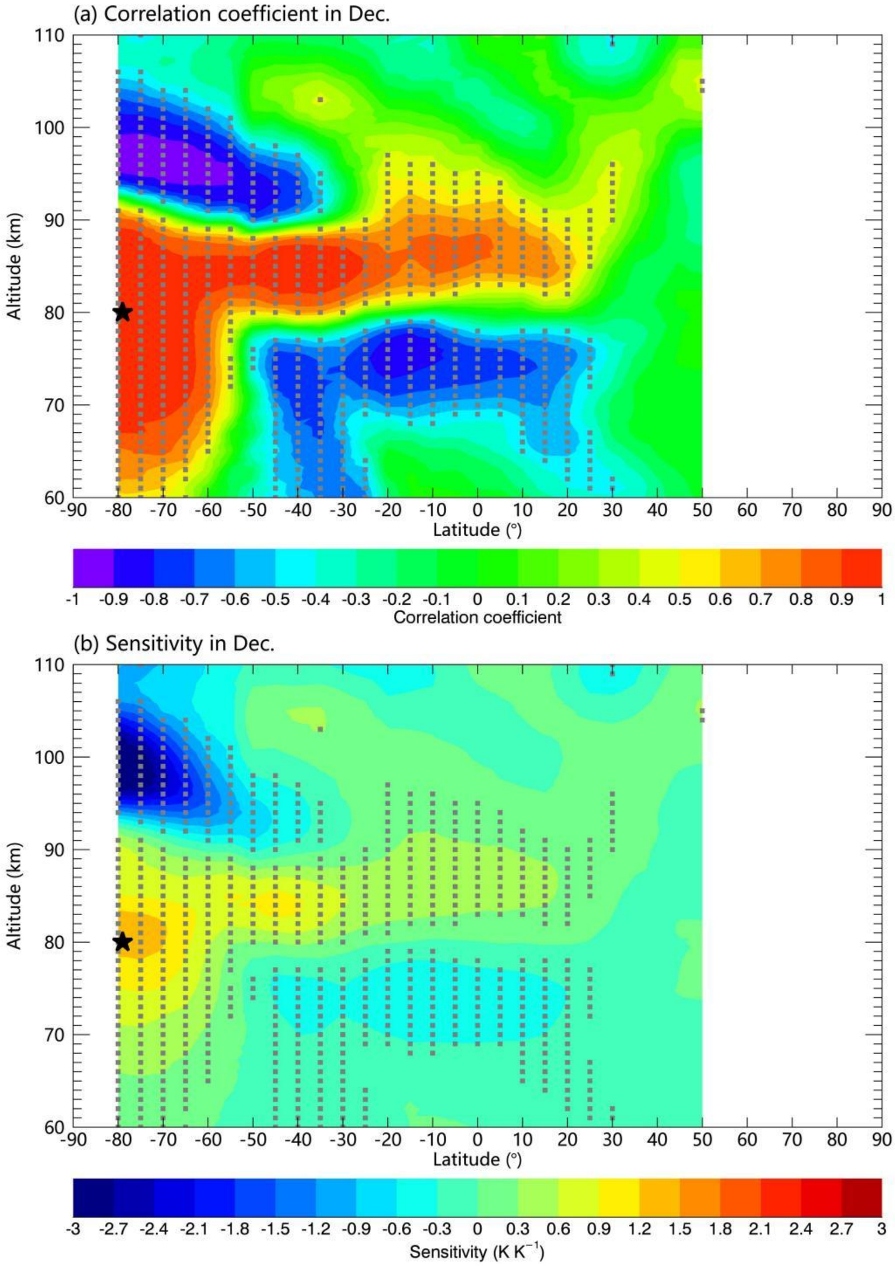

295 **Figure 11.** Latitudinal structure of the T80-temperature relationship in December. (a) The correlation coefficient and (b) the sensitivity between the T80 index and temperature at varying latitudes. Gray points mark the 0.95 significant level. Sensitivity is obtained by linear regression. All data are monthly and zonal means from SABER observation during 2002-2025.

https://doi.org/10.5194/egusphere-2026-4809
Preprint. Discussion started: 20 August 2026

4.3 Detectability of solar and CO_2 signals in MLT density

To isolate external forcing signals (11-year solar cycle and long-term CO_2 cooling) from internal dynamical variability controlled by polar upwelling, we quantify the solar response and secular linear trends of December MLT density across the full analysis domain. The solar radiation flux at 10.7 cm (f10.7, in units of sfu = 10^{-22} Wm^{-2} Hz^{-1}) is used as a proxy for solar activity (Tapping, 2013). The correlation coefficient between December T80 index and f10.7 during 2002-2025 is only R = 0.16 (fails the 95% significance test); therefore, they are independent.

Figure 12 shows the spatial structure of the MLT density response to f10.7 flux and the long-term linear trend of density. Fig. 12a reveals a clear spatial separation between solar signals and T80-driven density variability. Statistically significant correlations between f10.7 and December MLT density are confined to altitudes above 90 km within the broad latitudinal band of 50°S-50°N. By contrast, no significant solar cycle signal emerges below 100 km over southern high latitudes (60°S-80°S). Critically, the high-latitude MLT region where the T80 index exhibits its strongest density correlations (Fig. 4) lacks any detectable solar signature, demonstrating that internal polar upwelling dynamics overwhelm solar radiative forcing in modulating high-latitude summer MLT density on interannual timescales.

Figure 12b demonstrates the linear long-term trends of December MLT density. A positive trend appears near 80°S, 96 km, which seems contradictory to the canonical expectation of CO_2-driven atmospheric contraction and decreasing density. This apparent inconsistency is resolved by the dominant role of summer polar upwelling in governing high-latitude MLT column evolution. Over the 24-year record, the T80 index exhibits a positive linear trend (Fig. 2), indicating a gradual weakening of summer polar upwelling. A weaker upwelling reduces mesospheric adiabatic cooling and drives net expansion of the high-latitude atmospheric column, elevating the density at 96 km and producing the observed positive secular trend.

Collectively, these results demonstrate that neither 11-year solar activity nor long-term CO_2 radiative cooling can be reliably isolated from austral summer MLT density variations using the 2002-2025 SABER dataset. Internal dynamical perturbations of summer polar upwelling dominate both interannual and secular MLT density variability, fully obscuring weak external radiative forcing signals across the key high-latitude MLT layer modulated by the T80 index.

https://doi.org/10.5194/egusphere-2026-4809
Preprint. Discussion started: 20 August 2026

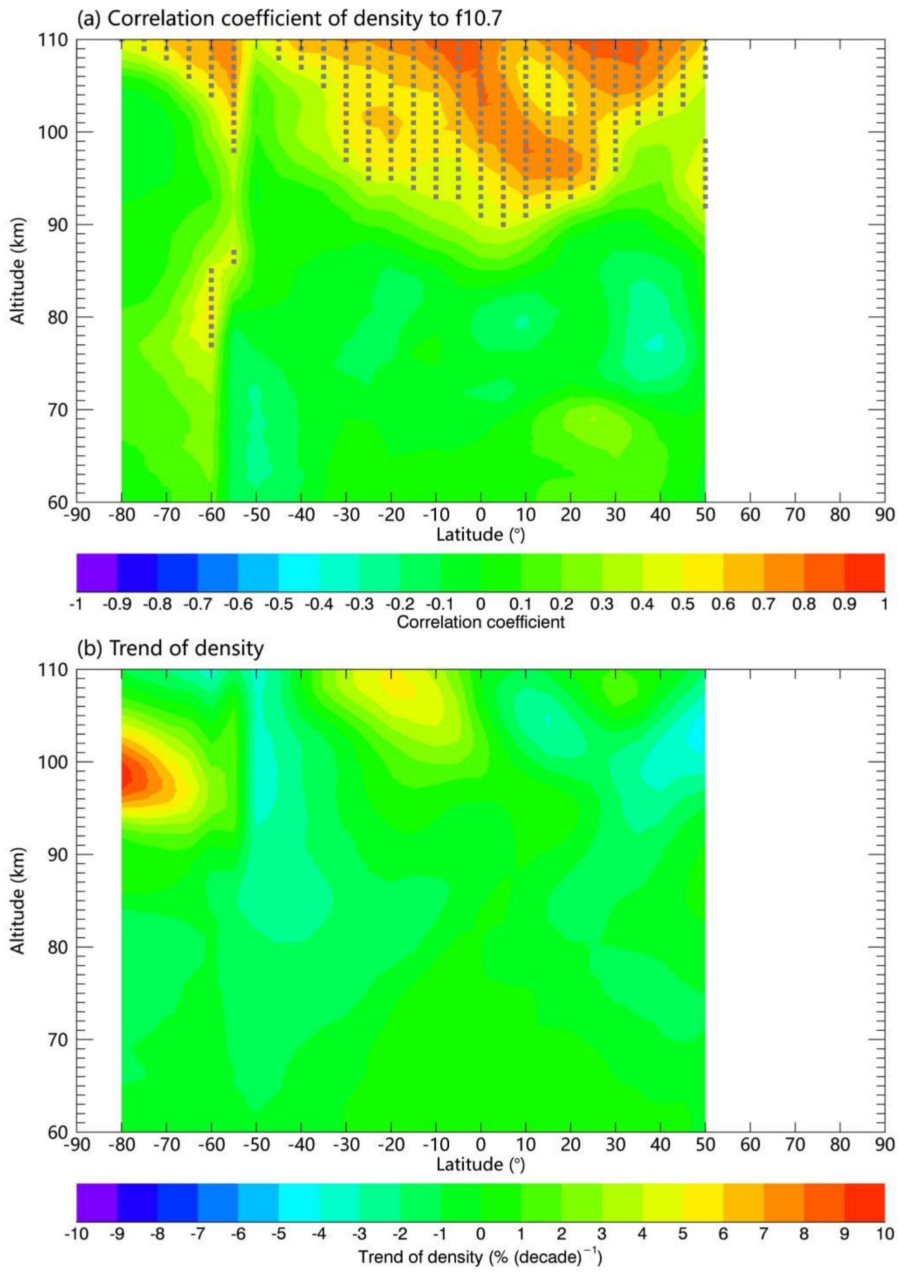

Figure 12. Influence of 11-year solar cycle on December MLT density and its long-term trends. (a) Correlation coefficient between density and the f10.7 index. Gray points mark the 95% significant level. (b) Linear trend of December MLT density.

https://doi.org/10.5194/egusphere-2026-4809
Preprint. Discussion started: 20 August 2026

4.4 Limitations and open questions

Several limitations and open questions should be acknowledged. First, our analysis is restricted to the SH summer months (November-January). For the NH summer months (May-July), our preliminary analysis suggests a similar but interhemispherically asymmetric relationship, which will be explored in a separate paper.

The CO_2-driven contraction signal during December is not yet separable from the dominant interannual variability within the current 24-year record. Although the role of CO_2 in driving long-term mesospheric contraction is widely recognized, extracting this signal during summer months requires longer observational records (multiple decades) and careful separation of radiative contributions (solar f10.7 and CO_2) from the dynamical contribution (T80 index). The present 24-year window is insufficient for this purpose. Importantly, this work does not challenge the well-established CO_2-driven contraction on annual-mean scales; rather, it demonstrates that polar upwelling variability masks this long-term contraction trend during austral summer months.

The high-latitude MLT density in the austral summer hemisphere is primarily driven by summer polar upwelling, therefore other MLT phenomena that depend on the ambient density profile (i.e., metal layer heights, meteoric peaking heights, and standard phase heights) should also covary with the T80 index on interannual timescales. Analyzing these MLT phenomena would be a necessary next step to validate the main findings of this work. Moreover, meteor radar networks provide reliable density observations between 85 and 95 km, offering an independent data source for cross-validation, which should be a priority for future research.

5 Conclusion

Using 24 years (2002-2025) of SABER temperature measurements, this study demonstrates that MLT density during austral summer months is predominantly controlled by the T80 index, a temperature-based proxy for the strength of summer polar upwelling. The major scientific findings are summarized as follows.

On interannual timescales, the T80 index dominates December MLT density variability across southern high latitudes (50°S-80°S). The covariation reaches a correlation coefficient of $R = 0.98$, with a linear density sensitivity of 3.1% K^{-1} near 95 km at 80°S. This robust T80-density linkage persists throughout the austral summer (November, December, and January). Significant coupling also exists on daily timescales, with a multi-year mean daily correlation coefficient of 0.78, although robust daily covariability is largely confined poleward of 50°S.

Two physical processes, the column adjustment effect and the local thermal effect, act competitively and cooperatively to shape the latitude-altitude pattern of density responses to T80 perturbations. Over southern high latitudes, these two mechanisms produce a distinct vertical density dipole. In the transitional layer of 85-91 km, the column adjustment effect counteracts the local thermal effect and dominates net density variations, generating an anomalous positive correlation between local temperature and density. At the upper MLT between 93-105 km, the two mechanisms operate synergistically, amplifying the extreme sensitivity of high-latitude density to polar upwelling anomalies. Meanwhile, enhanced polar

https://doi.org/10.5194/egusphere-2026-4809
Preprint. Discussion started: 20 August 2026

upwelling drives equatorward transport of H_2O, reducing O_x concentrations and lowering the temperature at low latitudes, thereby increasing low-latitude density between 80-90 km. Consequently, the summer polar upwelling drives interhemispheric anti-phase density variability through the bottom-up mechanism, analogous to the previously identified temperature pattern during austral summer (Zhang *et al.*, 2025c).

Owing to the strong month-to-month persistence of the T80 index during austral summer, skillful one-month-lead statistical forecasts of MLT density anomalies can be constructed using preceding T80 values. The November T80 index serves as a reliable predictor for December density, and the December T80 yields robust forecasts for January density. The maximum predictive correlation reaches 0.90 at 80°S, 96 km.

Further diagnosis of external radiative forcing signals reveals that neither the 11-year solar cycle nor long-term CO_2-driven cooling can be cleanly separated from internal dynamical variability within the 24-year SABER dataset. Detectable f10.7-density correlations only emerge above 90 km at mid and low latitudes, whereas solar signatures are negligible within the T80-controlled high-latitude MLT. For long-term trends, interannual dynamical fluctuations overwhelm secular linear trends. The positive density trend observed at 80°S, 95 km appears inconsistent with the canonical expectation of CO_2-induced atmospheric contraction. This counterintuitive trend originates from the gradual weakening of summer polar upwelling over the study period, which expands the high-latitude atmospheric column via the column adjustment effect. Accordingly, internal polar upwelling variability masks weak external radiative forcing signals in the high-latitude MLT region.

Overall, this work establishes the T80 index as a powerful diagnostic and predictive tool for austral summer MLT density. The influence of summer polar upwelling on MLT density through the bottom-up mechanism highlights the necessity of incorporating fully coupled dynamical, microphysical, chemical, and thermal processes into future MLT research.

Data Availability. The MLS Level 2, version 5 data are available for download from the NASA GES DISC website, with the temperature data accessible at https://disc.gsfc.nasa.gov/datasets/ML2T_005/summary. The MLS data quality document is available at https://mls.jpl.nasa.gov/data/v5-0_data_quality_document.pdf. The SABER data version 2.07 of temperature can be downloaded from https://data.gats-inc.com/saber/custom/Temp_O3_H2O/v2.0/. The solar f10.7 data can be obtained at https://omniweb.gsfc.nasa.gov/form/dx1.html via the GSFC/SPDF OMNI web interface.

Author Contributions. Liang Zhang conceived the idea, analyzed the data, and drafted the manuscript. Zhongfang Liu revised the paper. Yajun Zhu revised the paper.

Competing Interests. The authors declare that they have no conflict of interests.

https://doi.org/10.5194/egusphere-2026-4809
Preprint. Discussion started: 20 August 2026

Acknowledgements. We are especially grateful to the MLS and SABER program for providing us with the long-range and high-quality data, and we further wish to acknowledge the OMNI group for providing high-quality solar f10.7 data.

Financial support. This research has been supported by the National Natural Science Foundation of China (42025602 and 41905059).

References

Baron, P., Ochiai, S., Dupuy, E., Larsson, R., Liu, H., Manago, N., Murtagh, D., Oyama, S., Sagawa, H., Saito, A., Sakazaki, T., Shiotani, M. and Suzuki, M. (2020), Potential for the measurement of mesosphere and lower thermosphere (MLT) wind, temperature, density and geomagnetic field with Superconducting Submillimeter-Wave Limb-Emission Sounder 2 (SMILES-2), Atmos. Meas. Tech., 13(1), 219-237, https://doi.org/10.5194/amt-13-219-2020.

Cheng, X., Yang, J., Xiao, C. and Hu, X. (2020), Density Correction of NRLMSISE-00 in the Middle Atmosphere (20–100 km) Based on TIMED/SABER Density Data, in Atmosphere, edited, p. 341, https://doi.org/10.3390/atmos11040341.

Dawkins, E. C. M., Stober, G., Janches, D., Carrillo-Sánchez, J. D., Lieberman, R. S., Jacobi, C., Moffat-Griffin, T., Mitchell, N. J., Cobbett, N., Batista, P. P., Andrioli, V. F., Buriti, R. A., Murphy, D. J., Kero, J., Gulbrandsen, N., Tsutsumi, M., Kozlovsky, A., Kim, J. H., Lee, C. and Lester, M. (2023), Solar Cycle and Long-Term Trends in the Observed Peak of the Meteor Altitude Distributions by Meteor Radars, Geophysical Research Letters, 50(2), e2022GL101953, https://doi.org/10.1029/2022GL101953.

Emmert, J. T., Drob, D. P., Picone, J. M., Siskind, D. E., Jones Jr, M., Mlynczak, M. G., Bernath, P. F., Chu, X., Doornbos, E., Funke, B., Goncharenko, L. P., Hervig, M. E., Schwartz, M. J., Sheese, P. E., Vargas, F., Williams, B. P. and Yuan, T. (2021), NRLMSIS 2.0: A Whole-Atmosphere Empirical Model of Temperature and Neutral Species Densities, Earth and Space Science, 8(3), e2020EA001321, https://doi.org/10.1029/2020EA001321.

Feofilov, A. G. and Kutepov, A. A. (2012), Infrared Radiation in the Mesosphere and Lower Thermosphere: Energetic Effects and Remote Sensing, Surveys in Geophysics, 33(6), 1231-1280, https://doi.org/10.1007/s10712-012-9204-0.

García-Comas, M., Funke, B., Gardini, A., López-Puertas, M., Jurado-Navarro, A., von Clarmann, T., Stiller, G., Kiefer, M., Boone, C. D., Leblanc, T., Marshall, B. T., Schwartz, M. J. and Sheese, P. E. (2014), MIPAS temperature from the stratosphere to the lower thermosphere: Comparison of vM21 with ACE-FTS, MLS, OSIRIS, SABER, SOFIE and lidar measurements, Atmos. Meas. Tech., 7(11), 3633-3651, https://doi.org/10.5194/amt-7-3633-2014.

Garcia, R. R. and Solomon, S. (1985), The effect of breaking gravity waves on the dynamics and chemical composition of the mesosphere and lower thermosphere, Journal of Geophysical Research: Atmospheres, 90(D2), 3850-3868, https://doi.org/10.1029/JD090iD02p03850.

Holton, J. R. (1983), The Influence of Gravity Wave Breaking on the General Circulation of the Middle Atmosphere, Journal of Atmospheric Sciences, 40(10), 2497-2507, https://doi.org/10.1175/1520-0469(1983)040<2497:TIOGWB>2.0.CO;2.

Huang, N., Li, J., Lu, J., Fu, S., Sun, M., Wei, G., Zhan, M., Wang, M. and Xiong, S. (2025), Mesosphere and Lower Thermosphere (MLT) Density Responses to the May 2024 Superstorm at Mid-to-High Latitudes in the Northern Hemisphere Based on Sounding of the Atmosphere Using Broadband Emission Radiometry (SABER) Observations, in Remote Sensing, edited, p. 511, https://doi.org/10.3390/rs17030511.

Jiang, Y. B., Froidevaux, L., Lambert, A., Livesey, N. J., Read, W. G., Waters, J. W., Bojkov, B., Leblanc, T., McDermid, I. S., Godin-Beekmann, S., Filipiak, M. J., Harwood, R. S., Fuller, R. A., Daffer, W. H., Drouin, B. J., Cofield, R. E.,

https://doi.org/10.5194/egusphere-2026-4809
Preprint. Discussion started: 20 August 2026

Cuddy, D. T., Jarnot, R. F., Knosp, B. W., Perun, V. S., Schwartz, M. J., Snyder, W. V., Stek, P. C., Thurstans, R. P., Wagner, P. A., Allaart, M., Andersen, S. B., Bodeker, G., Calpini, B., Claude, H., Coetzee, G., Davies, J., De Backer, H., Dier, H., Fujiwara, M., Johnson, B., Kelder, H., Leme, N. P., König-Langlo, G., Kyro, E., Laneve, G., Fook, L. S., Merrill, J., Morris, G., Newchurch, M., Oltmans, S., Parrondos, M. C., Posny, F., Schmidlin, F., Skrivankova, P., Stubi, R., Tarasick, D., Thompson, A., Thouret, V., Viatte, P., Vömel, H., von Der Gathen, P., Yela, M. and Zablocki, G. (2007), Validation of Aura Microwave Limb Sounder Ozone by ozonesonde and lidar measurements, Journal of Geophysical Research: Atmospheres, 112(D24), https://doi.org/10.1029/2007JD008776.

Laštovička, J. (2017), A review of recent progress in trends in the upper atmosphere, Journal of Atmospheric and Solar-Terrestrial Physics, 163, 2-13, https://doi.org/10.1016/j.jastp.2017.03.009.

Li, J., Zhang, X., Fu, S., Li, G., Tian, Y., Li, C., Wang, Z., Lu, J., Wang, M., Li, Z., Zhang, H., Yao, H., Li, S., Sun, X., Huang, N., Wei, G. and Zhan, M. (2025), Equatorial Anomalous Responses of the Mesosphere and Lower Thermosphere Temperature to Super Geomagnetic Storms Observed by TIMED/SABER, Geophysical Research Letters, 52(17), e2025GL114776, https://doi.org/10.1029/2025GL114776.

Li, Z., Chen, X., Zhang, H., Li, J. and Sun, Y. (2026), The Prediction of Short-Term Atmospheric Density in Lower Thermosphere, Space Weather, 24(4), e2025SW004896, https://doi.org/10.1029/2025SW004896.

Lindzen, R. S. (1981), Turbulence and stress owing to gravity wave and tidal breakdown, Journal of Geophysical Research, 86(C10), 9707-9714, https://doi.org/10.1029/JC086iC10p09707.

Liu, X., Xu, J., Yue, J., Wang, W. and Moro, J. (2025), Mesosphere and Lower Thermosphere Temperature Responses to the May 2024 Mother's Day Storm, Geophysical Research Letters, 52(2), e2024GL112179, https://doi.org/10.1029/2024GL112179.

Liu, X., Xu, J., Yue, J., Yuan, T., She, C. Y. and Vital, L. F. R. (2026), Assessments the Long-Term Stability of the SABER Temperature Measurement in the Middle Latitude MLT Region, Journal of Geophysical Research: Space Physics, 131(4), e2025JA034476, https://doi.org/10.1029/2025JA034476.

Lübken, F.-J., Berger, U. and Baumgarten, G. (2013), Temperature trends in the midlatitude summer mesosphere, Journal of Geophysical Research: Atmospheres, 118(24), 13,347-13,360, https://doi.org/10.1002/2013JD020576.

Mlynczak, M. G., Daniels, T., Hunt, L. A., Yue, J., Marshall, B. T., Russell Iii, J. M., Remsberg, E. E., Tansock, J., Esplin, R., Jensen, M., Shumway, A., Gordley, L. and Yee, J. H. (2020), Radiometric Stability of the SABER Instrument, Earth and Space Science, 7(2), e2019EA001011, https://doi.org/10.1029/2019EA001011.

Mlynczak, M. G., Hunt, L. A., Garcia, R. R., Harvey, V. L., Marshall, B. T., Yue, J., Mertens, C. J. and Russell III, J. M. (2022), Cooling and Contraction of the Mesosphere and Lower Thermosphere From 2002 to 2021, Journal of Geophysical Research: Atmospheres, 127(22), e2022JD036767, https://doi.org/10.1029/2022JD036767.

Peters, D. H. W., Entzian, G. and Keckhut, P. (2017), Mesospheric temperature trends derived from standard phase-height measurements, Journal of Atmospheric and Solar-Terrestrial Physics, 163, 23-30, https://doi.org/10.1016/j.jastp.2017.04.007.

Plane, J. M. C., Gumbel, J., Kalogerakis, K. S., Marsh, D. R. and von Savigny, C. (2023), Opinion: Recent developments and future directions in studying the mesosphere and lower thermosphere, Atmospheric Chemistry and Physics, 23(20), 13255-13282, https://doi.org/10.5194/acp-23-13255-2023.

Remsberg, E. E., Marshall, B. T., Garcia-Comas, M., Krueger, D., Lingenfelser, G. S., Martin-Torres, J., Mlynczak, M. G., Russell Iii, J. M., Smith, A. K., Zhao, Y., Brown, C., Gordley, L. L., Lopez-Gonzalez, M. J., Lopez-Puertas, M., She, C. Y., Taylor, M. J. and Thompson, R. E. (2008), Assessment of the quality of the Version 1.07 temperature-versus-pressure profiles of the middle atmosphere from TIMED/SABER, Journal of Geophysical Research: Atmospheres, 113(D17), https://doi.org/10.1029/2008JD010013.

https://doi.org/10.5194/egusphere-2026-4809
Preprint. Discussion started: 20 August 2026

Roble, R. G. and Dickinson, R. E. (1989), How will changes in carbon dioxide and methane modify the mean structure of the mesosphere and thermosphere?, Geophysical Research Letters, 16(12), 1441-1444, https://doi.org/10.1029/GL016i012p01441.

Russell, J., Mlynczak, M., Gordley, L., Tansock, J. and Esplin, R. (1999), Overview of the SABER experiment and preliminary calibration results, SPIE Proceedings, 3756(20), 277-288, https://doi.org/10.1117/12.366382.

Schwartz, M. J., Lambert, A., Manney, G. L., Read, W. G., Livesey, N. J., Froidevaux, L., Ao, C. O., Bernath, P. F., Boone, C. D., Cofield, R. E., Daffer, W. H., Drouin, B. J., Fetzer, E. J., Fuller, R. A., Jarnot, R. F., Jiang, J. H., Jiang, Y. B., Knosp, B. W., Krüger, K., Li, J. L. F., Mlynczak, M. G., Pawson, S., Russell Iii, J. M., Santee, M. L., Snyder, W. V., Stek, P. C., Thurstans, R. P., Tompkins, A. M., Wagner, P. A., Walker, K. A., Waters, J. W. and Wu, D. L. (2008), Validation of the Aura Microwave Limb Sounder temperature and geopotential height measurements, Journal of Geophysical Research: Atmospheres, 113(D15), https://doi.org/10.1029/2007JD008783.

She, C.-Y., Berger, U., Yan, Z.-A., Yuan, T., Lübken, F. J., Krueger, D. A. and Hu, X. (2019), Solar Response and Long-Term Trend of Midlatitude Mesopause Region Temperature Based on 28 Years (1990–2017) of Na Lidar Observations, Journal of Geophysical Research: Space Physics, 124(8), 7140-7156, https://doi.org/10.1029/2019JA026759.

Siskind, D. E., Merkel, A. W., Marsh, D. R., Randall, C. E., Hervig, M. E., Mlynczak, M. G. and Russell Iii, J. M. (2018), Understanding the Effects of Polar Mesospheric Clouds on the Environment of the Upper Mesosphere and Lower Thermosphere, Journal of Geophysical Research: Atmospheres, 123(20), 11,705-11,719, https://doi.org/10.1029/2018JD028830.

Smith, A. K. (2012), Global Dynamics of the MLT, Surveys in Geophysics, 33(6), 1177-1230, https://doi.org/10.1007/s10712-012-9196-9.

Sun, M., Lu, J., Li, J., Wei, G., Li, Z., Huang, N. and Zhan, M. (2025), Responses of High-Latitude Mesopause Height and Temperature to Geomagnetic Storms, Journal of Geophysical Research: Space Physics, 130(4), e2024JA033624, https://doi.org/10.1029/2024JA033624.

Tapping, K. F. (2013), The 10.7 cm solar radio flux (F10.7), Space Weather, 11(7), 394-406, https://doi.org/10.1002/swe.20064.

Vincent, R. A. (2015), The dynamics of the mesosphere and lower thermosphere: a brief review, Progress in Earth and Planetary Science, 2(1), 4, https://doi.org/10.1186/s40645-015-0035-8.

Wang, Z., Xiao, C., Hu, X., Yang, J., Cheng, X., Li, K., Xiao, L., Wu, X., Yu, Y. and Li, H. (2025), A New Method for Determining the Wave Turbopause Based on SABER/TIMED Data, in Remote Sensing, edited, p. 623, https://doi.org/10.3390/rs17040623.

Wu, X., Zhu, Y., Smith, A. K., Kaufmann, M., Jiang, G., Liu, S. and Xu, J. (2026), A new data set of nighttime chemical heating rates in the upper mesosphere and lower thermosphere derived from SCIAMACHY OH (9–6) emissions and SABER profiles, Atmos. Chem. Phys., 26(7), 4669-4683, https://doi.org/10.5194/acp-26-4669-2026.

Yang, J., Wang, J., Liu, D., Guo, W. and Zhang, Y. (2024), Observation and simulation of neutral air density in the middle atmosphere during the 2021 sudden stratospheric warming event, Atmos. Chem. Phys., 24(17), 10113-10127, https://doi.org/10.5194/acp-24-10113-2024.

Yi, W., Reid, I. M., Xue, X., Murphy, D. J., Hall, C. M., Tsutsumi, M., Ning, B., Li, G., Younger, J. P., Chen, T. and Dou, X. (2018a), High- and Middle-Latitude Neutral Mesospheric Density Response to Geomagnetic Storms, Geophysical research letters, 45(1), 436-444, https://doi.org/10.1002/2017GL076282.

Yi, W., Reid, I. M., Xue, X., Younger, J. P., Murphy, D. J., Chen, T. and Dou, X. (2017a), Response of neutral mesospheric density to geomagnetic forcing, Geophysical research letters, 44(16), 8647-8655, https://doi.org/10.1002/2017GL074813.

https://doi.org/10.5194/egusphere-2026-4809
Preprint. Discussion started: 20 August 2026

Yi, W., Reid, I. M., Xue, X., Younger, J. P., Spargo, A. J., Murphy, D. J., Chen, T. and Dou, X. (2017b), First observation of mesosphere response to the solar wind high-speed streams, Journal of Geophysical Research:Space Physics, 122(8), 9080-9088, https://doi.org/10.1002/2017JA024446.

Yi, W., Xue, X., Lu, M., Zeng, J., Ye, H., Wu, J., Wang, C. and Chen, T. (2023), Mesopause temperatures and relative densities at midlatitudes observed by the Mengcheng meteor radar, Earth and Planetary Physics, 7(6), 665-674, https://doi.org/10.26464/epp2023083.

Yi, W., Xue, X., Reid, I. M., Murphy, D. J., Hall, C. M., Tsutsumi, M., Ning, B., Li, G., Vincent, R. A., Chen, J., Wu, J., Chen, T. and Dou, X. (2019), Climatology of the mesopause relative density using a global distribution of meteor radars, Atmos. Chem. Phys., 19(11), 7567-7581, https://doi.org/10.5194/acp-19-7567-2019.

Yi, W., Xue, X., Reid, I. M., Younger, J. P., Chen, J., Chen, T. and Li, N. (2018b), Estimation of Mesospheric Densities at Low Latitudes Using the Kunming Meteor Radar Together With SABER Temperatures, Journal of Geophysical Research:Space Physics, 123(4), 3183-3195, https://doi.org/10.1002/2017JA025059.

Younger, J. P., Reid, I. M., Vincent, R. A. and Murphy, D. J. (2015), A method for estimating the height of a mesospheric density level using meteor radar, Geophysical Research Letters, 42(14), 6106-6111, https://doi.org/10.1002/2015GL065066.

Zhang, L. and Liu, Z. (2026), A Triple-Structured Mesospheric Climate Pattern Driven by a Double-Celled Meridional Circulation during the Equinox-Solstice Transition Months of November and May, EGUsphere, 2026, 1-32, https://doi.org/10.5194/egusphere-2026-2688.

Zhang, L., Liu, Z. and Tinsley, B. (2025a), Altitude-dependent formation of polar mesospheric clouds: charged nucleation and in situ ice growth on zonal and daily scales, Atmos. Chem. Phys., 25(19), 12701-12719, https://doi.org/10.5194/acp-25-12701-2025.

Zhang, L., Liu, Z. and Tinsley, B. (2025b), Height-Latitude Patterns of Interannual Climate Variability in the Upper Mesosphere and Lower Thermosphere During Spring and Autumn Months, Geophysical Research Letters, 52(13), e2025GL116281, https://doi.org/10.1029/2025GL116281.

Zhang, L., Liu, Z. and Tinsley, B. (2025c), Interhemispheric Anti-Phase Variability in Mesospheric Climate Driven by Summer Polar Upwelling During Solstice Months, Atmos. Chem. Phys., 25(20), 13141-13159, https://doi.org/10.5194/acp-25-13141-2025.

Zhang, L., Liu, Z. and Zhu, Y. (2026), Quantifying and Predicting Austral Summer Mesopause Height with a Temperature-Based Upwelling Proxy, EGUsphere, 2026, 1-28, https://doi.org/10.5194/egusphere-2026-3749.

Zhang, L., Tinsley, B. and Zhou, L. (2022), Responses of CIPS/AIM noctilucent clouds to the interplanetary magnetic field, Atmospheric Chemistry and Physics, 22(20), 13355-13370, https://doi.org/10.5194/acp-22-13355-2022.

Zhao, X. R., Sheng, Z., Shi, H. Q., Weng, L. B. and Liao, Q. X. (2020), Long-Term Trends and Solar Responses of the Mesopause Temperatures Observed by SABER During the 2002–2019 Period, Journal of Geophysical Research: Atmospheres, 125(11), e2020JD032418, https://doi.org/10.1029/2020JD032418.